Comparison of Free-Flight Experimental Results with Theory on the Nonlinear Aerodynamic Effects of Bluntness for Slender Cones at Mach Number 17

GERALD N. MALCOLM* AND JOHN V. RAKICH†
NASA Ames Research Center, Moffett Field, Calif.

Free-flight tests of 12.5° half-angle cones with bluntness ratios (nose radius to base radius) from 0 to 0.5 have been conducted at Mach numbers 17 to 18. Conventional wind-tunnel tests were also conducted on 10° half-angle cones with bluntness ratios from 0 to 0.25 at Mach 10.6. Results from both of these tests are compared to recent theoretical calculations as well as to existing theories and data. The results show that the strong dependence of initial moment-curve slope on nose bluntness known to occur for Mach numbers near 10 is found to be even more pronounced at M = 17. This effect is accurately predicted by recent theoretical calculations using method of characteristics both at zero angle of attack and angles up to 5°. Other theoretical results are also shown which give good agreement, including Ericsson's theory based on the embedded Newtonian flow concept and Clay and Walchner's empirical correlation. The present paper shows, in addition, that strong nonlinearities in the pitching moment occur with angle of attack which tend to decrease stability with increasing angle for small nose bluntness and increase stability with increasing angle for large nose bluntness. Experimental results and some comparisons with theory are also presented for normal force and center-of-pressure location.

Nomenclature

A = reference area (model base area)
C_m = pitching-moment coefficient
C_{m_α} = pitching-moment-coefficient slope, $\partial C_m/\partial\alpha$ at $\alpha = 0°$
$C_{m_{\alpha_l}}$ = quasi-linear pitching-moment-curve slope, Eq. (3)
C_{N_α} = normal-force-curve slope
d = reference length (model base diameter)
I_y = moment of inertia about a transverse axis through the center of gravity
$K_{1,2,3}$ = constants in Eq. (1)
l = model length
l_c = virtual length (length of basic sharp cone)
M = Mach number
p = roll rate about axis of symmetry of model
R = Reynolds number based on freestream conditions and cone virtual length l_c
r_b = model base radius
r_n = nose radius
x = distance flown
x_{cg} = axial distance from model base to center of gravity
x_{cp} = axial distance from model base to center of pressure
α = angle of attack (in the vertical plane)
α_m = average maximum resultant angle of attack
$\alpha_{\min}$ = average minimum resultant angle of attack
β = angle of sideslip (in the horizontal plane)
$\eta_{1,2}$ = damping exponents in Eq. (1)
λ = wavelength of pitching oscillation
ρ = freestream air density
$\omega_{1,2}$ = rates of rotation of vectors that describe the model oscillatory motion in Eq. (1)

Introduction

DURING the last few years aerodynamicists have observed that a small amount of nose blunting can have a significant effect on the static and dynamic stability of slender cones at hypersonic speeds. Newtonian theory, which has provided many insights into hypersonic aerodynamics, does not predict this effect. Other theoretical methods have been developed, however, to attempt to explain the observations.

The first definitive treatment of static and dynamic stability of slightly blunted slender cones was given by Clay and Walchner.[1-3] They developed an approximate analytical method based on an empirical correlation[4] of the zero-lift pressure distribution on blunted cones with Cheng's[5] distance parameter. Reasonably good agreement with experimental results was obtained for the static-stability rise with bluntness but not the change in dynamic stability. A better analytical prediction of the dynamic stability and a comparably accurate prediction of the static stability was obtained by Ericsson,[6,7] using embedded Newtonian concepts originally developed by Seiff.[8] This method attempts to account for the loss of dynamic pressure on the afterbody which results from the strong shock (blast) wave created by the blunt nose. For unsteady cases, it also takes into account the time lag before a translatory movement of the nose results in translation of the inviscid shear-flow profile to downstream body elements. Exact numerical results have also been obtained for the static stability at zero angle of attack by Rakich[9] and for both static and dynamic stability by Brong[10] and Rie, et al.[11] The numerical methods develop the angle of attack or unsteady flowfield as a small perturbation of the exact nonlinear zero angle-of-attack flow. They properly account for both the overexpansion of the bow shock and the loss of dynamic pressure in the entropy layer which envelops the afterbody.

The approximate methods described have been shown[2,7,12] to provide reasonably good estimates of static stability at Mach numbers of 10 and 14. However, significant Mach number effects not predicted by the approximate methods (which are essentially independent of Mach number) have been found by recent calculations with the exact numerical method of Ref. 9. This effect was corroborated by a small amount of data available from tests in the Ames Supersonic Free-Flight Wind Tunnel (SSFF) in 1963. Figure 1 shows experimental and theoretical results for 12.5° blunted cones at Mach 10 and 17 and includes a comparison with Newtonian theory. Small perturbation theory indicates a difference in static stability due to Mach number of approximately 25% for bluntness ratios near 0.17. Comparison of the three

Presented as Paper 70-554 at the AIAA Atmospheric Flight Mechanics Conference, Tullahoma, Tenn., May 13-15, 1970; submitted June 1, 1970; revision received September 30, 1970.
* Research Scientist. Member AIAA.
† Research Scientist. Associate Fellow AIAA.

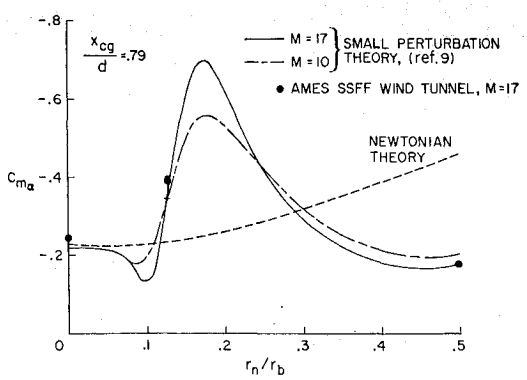

Fig. 1 Theoretical calculations of static stability coefficient at $\alpha = 0°$ for blunted 12.5° cones.

experimental points with the $M = 17$ theory showed such good agreement that further tests at Mach 17 for other bluntness ratios seemed desirable.

The present work was therefore undertaken to test the theoretical calculations and to investigate the dependence on Mach number. Additional free-flight tests were performed, and since the original SSFF Wind Tunnel was no longer operational, they were conducted in the Ames Hypervelocity Free-Flight Aerodynamic Facility (AHFF), a ballistic facility with 16 shadowgraph stations spaced at 1.52 meter intervals. Models were gun-launched into a shock-tube-driven countercurrent flow from a deformable-piston light-gas gun having a bore diameter of 2.54 cm.

In order to investigate the extremes of the theoretical curve for $M = 17$ in Fig. 1, tests were performed with cones of bluntness ratios $r_n/r_b = 0.09, 0.16, 0.20$, and 0.3. In addition, a limited number of tests with model bluntness ratios the same as those of the earlier tests shown in Fig. 1 ($r_n/r_b = 0, 0.125$, and 0.5) were performed to demonstrate repeatability of those results. Wind-tunnel tests with sting-mounted models were also performed in the Ames 3.5-Foot Hypersonic Wind Tunnel at Mach 10 on 10° cones ranging in bluntness ratio from 0.0 to 0.25. These data are compared to available theoretical and experimental results for 10° cones.

Although they will not be shown here, data were obtained for lift, drag, and dynamic stability from the free flight tests and are reported in Ref. 13.

Theoretical Calculations

The observed variations in static stability of blunted cones are caused mainly by the displacement of the bow shock wave due to the blunt nose.[9] The shock first over-corrects for the presence of the nose but then slowly approaches the shock position of the pointed cone far downstream from the nose. The numerical computation of such flows is difficult for small bluntness ratios. One must start with a solution for a spherical nose and calculate the flow along the afterbody for a distance of 100 to 200 nose radii. Care must therefore be taken to insure that numerical roundoff errors do not build up to destroy the over-all accuracy of the calculation.

Two different methods have been used for these calculations and are described here. The first is a small perturbation technique applicable near zero angle of attack, and the second is a general three-dimensional method of characteristics.

Small Angle of Attack

Methods employing a small perturbation in angle of attack have been well established for calculating force and moment derivatives at zero angle of attack. For nonconical bodies the method is also known as the linearized characteristics method (actually a misnomer). The exact nonlinear flow around the body at zero angle of attack is calculated and the perturbation field due to a small angle of attack is concurrently determined. The method therefore gives the "exact" derivative of the pressure, forces, and moments with respect to α at $\alpha = 0$. Of course, the degree of exactness depends on the size of the finite difference mesh used in the calculation. One difficulty associated with this method is that the characteristic network becomes very nonuniform far downstream from the nose. The mesh size becomes too coarse in regions of rarefaction and may cause an overprediction in the peak value of C_{m_α}.

Because of these inherent difficulties, calculations were performed with different mesh-point densities. It was found that 20 starting points on the spherical nose were needed to obtain a converged solution for a bluntness of about $r_n/r_b = 0.16$. Numerical results from this small perturbation method were shown in Fig. 1, and will be compared with the static-stability results at $\alpha = 0$ obtained from the present free-flight experiments. For angles of attack greater than zero, a different method is required and is described next.

Large Angles of Attack

The general three-dimensional program for large angles of attack is a more recent development,[14] and is a complete departure from the small perturbation method. The new method maintains a uniform distribution of mesh points and, therefore, a better control of accuracy. However, this program is more time-consuming since the calculations are performed on several planes spaced around the body. The time for the computations is typically about 30 min per case on an IBM 360-67. Some results are shown later in the paper and were obtained with 15 mesh points between the body and shock wave on each of 7 meridional planes.

Free-Flight Tests

Test Conditions

Models were gun-launched at a nominal velocity of 1980 m/sec into a countercurrent airstream with a velocity of 1370 m/sec for a combined velocity of 3350 m/sec. The freestream temperature was 83°K, which resulted in an average flight Mach number of 18. (Previous tests were at Mach numbers nearer 17; for simplicity all free-flight results will be referred to as Mach 17 results.) The Reynolds number based on cone virtual length l_c and freestream conditions was 1.35 million for the present tests, as compared to 5.6 million for the previous tests. The difference is principally caused by the lower freestream density required for the present tests. Angle and position measurements were made from the shadowgraph pictures to within 0.5° and 0.01 cm, respectively, and flight time at each station was recorded with electronic chronographs accurate to within 0.01 μsec.

Models

Models were either aluminum with hollowed bases or were bimetallic with steel noses and hollowed aluminum afterbodies. The center of gravity for all models was 0.35 l_c (0.79d) from the base, where l_c is the virtual cone length. Model diameter was 1.525 cm. Small steel pins were installed in the base to enable roll angles to be read from the shadowgraphs and the roll rate to be thereby determined.

Reduction of Data

The data-reduction techniques used to deduce the aerodynamic coefficients of static and dynamic stability, drag, and lift from free-flight data at the Hypersonic Free-Flight Branch of the Ames Research Center are presented in Ref. 15. Only the basic equations and a brief description of the techniques for extracting static stability data will be presented here.

Static-Stability Derivatives

The stability derivatives were determined from analysis of the pitching and yawing motions experienced by the models during free flight. The analysis consisted of fitting the following well-known tricyclic equation, derived by Nicolaides,[16] to the measurements of α and β of each flight:

$$\beta + i\alpha = K_1 e^{(\eta_1 + i\omega_1)x} + K_2 e^{(\eta_2 - i\omega_2)x} + K_3 e^{ipx} \quad (1)$$

where $\eta_{1,2}$ and $\omega_{1,2}$ are functions of the aerodynamic stability coefficients and $K_{1,2,3}$ are functions of the initial conditions. The most important assumptions inherent in this equation are linear aerodynamics (restrictions implied are discussed in the next paragraph), small angles of attack, constant roll rate, and small asymmetries. In the present analysis it was further assumed that the Magnus moment was zero. A least-squares procedure using differential corrections was used to determine optimum values of the constants. The static-stability parameter is related to the constants in Eq. (1), as follows. The wavelength of oscillation is given by

$$\lambda = 2\pi/(\omega_1\omega_2)^{1/2} \quad (2)$$

The quasi-linear pitching-moment-curve slope $C_{m_{\alpha_l}}$ is computed from the relation

$$C_{m_{\alpha_l}} = -8\pi^2 I_y/\lambda^2 \rho A d \quad (3)$$

Although the assumption of linear aerodynamics is inherent in Eq. (1), this does not prevent its use for bodies with nonlinear stability coefficients. Each individual flight is reduced as if the governing pitching moment were linear with angle of attack; the resulting wavelength of oscillation (which is necessarily constant) represents a quasi-linear value for the pitching-moment-curve slope or static stability. Quasi-linear values for static stability from several flights at various angle-of-attack amplitudes can be used to obtain the nonlinear pitching moment coefficient as a function of angle of attack. The method is derived in Ref. 17 and illustrated in some detail in Ref. 18. Basically, for a pitching moment equation of the form

$$-C_m = P_0\alpha + P_1\alpha^2 + P_2\alpha^3 + P_3\alpha^4 + P_4\alpha^5 + P_5\alpha^6 + P_6\alpha^7 \ldots \quad (4)$$

the equation for the quasi-linear value of the pitching-moment-curve slope $C_{m_{\alpha_l}}$ can be written

$$-C_{m_{\alpha_l}} = P_0 + (\tfrac{8}{3})P_1 b + (\tfrac{3}{4})P_2 c + (\tfrac{8}{5})P_3 d + (\tfrac{1}{12})P_4 e + (\tfrac{8}{7})P_5 f + (\tfrac{5}{32})P_6 g \ldots \quad (5)$$

where

$$b = \frac{(\alpha_m{}^5 + \alpha_{\min}{}^5)/2 - [(\alpha_m{}^2 + \alpha_{\min}{}^2)/2]^{5/2}}{(\alpha_m{}^2 - \alpha_{\min}{}^2)^2}$$

$$c = \alpha_m{}^2 + \alpha_{\min}{}^2$$

$$d = \frac{(\alpha_m{}^7 + \alpha_{\min}{}^7)/2 - [(\alpha_m{}^2 + \alpha_{\min}{}^2)/2]^{7/2}}{(\alpha_m{}^2 - \alpha_{\min}{}^2)^2}$$

$$e = 7\alpha_m{}^4 + 10\alpha_m{}^2\alpha_{\min}{}^7 + 7\alpha_{\min}{}^4$$

$$f = \frac{(\alpha_m{}^9 + \alpha_{\min}{}^9)/2 - [(\alpha_m{}^2 + \alpha_{\min}{}^2)/2]^{9/2}}{(\alpha_m{}^2 - \alpha_m{}^2)^2}$$

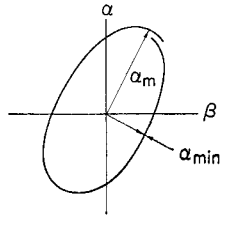

Fig. 2 Sketch of average maximum and minimum angles in the α-β plane.

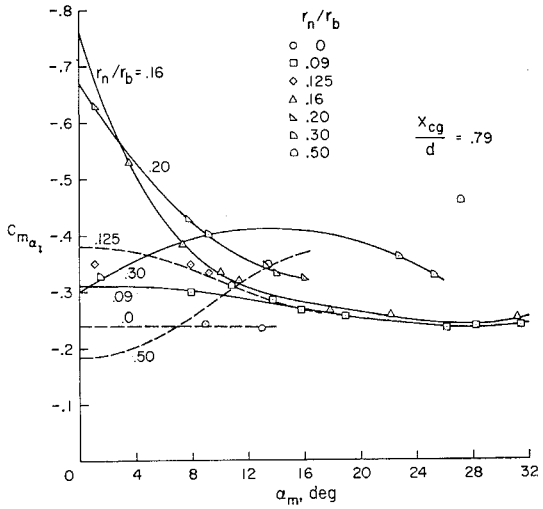

Fig. 3 Static stability coefficient vs average maximum angle of attack for blunt 12.5° cones at $M \approx 17$.

$$g = 3\alpha_m{}^6 + 5\alpha_m{}^4\alpha_{\min}{}^2 + 5\alpha_m{}^2\alpha_{\min}{}^4 + 3\alpha_{\min}{}^6$$

and α_m and $\alpha_{\min}$ are the average maximum and minimum resultant angles, respectively, in the $\alpha - \beta$ plane (see Fig. 2).

Values of $C_{m_{\alpha_l}}$, α_m, and $\alpha_{\min}$ from several flights are fitted by a least-squares procedure using as many terms of Eq. (5) as desired (a computer program has been written to accomplish this systematically[18]), and the resulting coefficients P_0, P_1, P_2, etc., are determined. These coefficients then produce an expression for C_m vs α.

Wind-Tunnel Tests

Wind-tunnel tests with sting-mounted models were conducted in the Ames 3.5-Foot Hypersonic Wind Tunnel on a series of 10° cones with bluntness ratios ranging from 0 to 0.25. The nominal Mach number was 10.6, and the nominal total temperature was 1100°K. The total pressure was varied between 27 and 109 atm to vary Reynolds number based on virtual length and free stream conditions from 0.18 to 1.3 million. Axial forces, normal forces, and pitching moments were measured with a three-component strain gage balance. Data were recorded at fixed time intervals as the models were slowly traversed through a complete angle-of-attack cycle between $\alpha = \pm 5°$. The time span for each one-cycle traverse was approximately 30 sec which allowed the recording of about 80 to 100 data points.

Models were constructed of aluminum with removable noses to provide convenient changes in nose bluntness. Two different model sizes were used with base diameters of 5.08 cm and 10.16 cm.

Experimental Free-Flight Results

Static Stability

The static-stability results of these tests are shown in Fig. 3, where the quasi-linear static-stability coefficient $C_{m_{\alpha_l}}$ is plotted vs the average maximum angle of attack of each flight. All the flights exhibited nearly pure pitching motions (i.e., $\alpha_{\min} \approx 0$). Each set of data points was fit with a polynomial, Eq. (5), as described earlier. [Note that since $\alpha_{\min} \approx 0$, Eq. (5) is nearly a polynomial in α_m alone and thereby justifies plotting $C_{m_{\alpha_l}}$ vs α_m.] The solid curves for $r_n/r_b = 0.09$, 0.16, 0.20, and 0.30 are fits to the present data. The dashed curves for $r_n/r_b = 0$, 0.125, and 0.50 are fits to the previous data, and the few new data points for these bluntnesses are shown for comparison. It is very apparent that there is a large variation of static stability near $\alpha_m = 0$ with

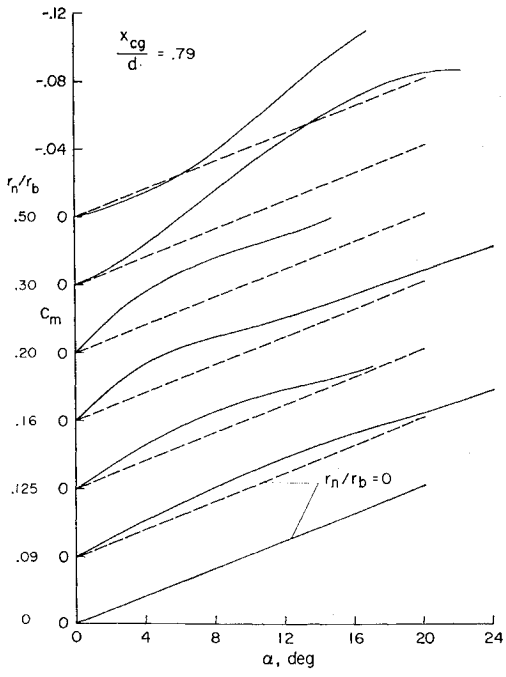

Fig. 4 Pitching-moment coefficient vs angle of attack for blunt 12.5° cones at $M \approx 17$.

bluntness and for most bluntness ratios the static stability is very nonlinear with angle of attack. Starting with the pointed cone, the zero-angle static stability increases with bluntness until $r_n/r_b = 0.16$ then decreases to a value below that of the pointed cone for $r_n/r_b = 0.5$. The zero-angle values will be compared later to the theoretical curve of C_{m_α} vs r_n/r_b. If we examine the nonlinearity of the static stability with angle of attack, we find that it varies greatly depending on bluntness. The pointed cone shows linear static stability in the small angle range, that is, C_{m_α} is constant with angle of attack. The curves for $r_n/r_b = 0.09$ and 0.125 indicate nonlinearities which are of similar nature to one another but differ slightly in magnitude. The curves for $r_n/r_b = 0.16$ and 0.20 are extremely nonlinear with the static stability being highest at $\alpha_m = 0$ and dropping rapidly with increasing angle of attack. The pattern of the nonlinearity changes for $r_n/r_b = 0.3$ and 0.5, with static stability initially *increasing* with angle of attack. The resulting variation of pitching moment coefficient with angle of attack for each of these seven bluntness ratios is shown in Fig. 4. The pointed cone curve is shown repeatedly for reference. In Fig. 5 the initial slopes of the pitching-moment curves, the zero-angle values of Fig. 3, are compared to small perturbation theory.[9] Excepting $r_n/r_b = 0.09$, there is good agreement between theory and experiment at all bluntness values tested including the maximum value near $r_n/r_b = 0.16$. The theory apparently underestimates the stability in the region between the pointed cone and the 12.5% blunt cone, probably

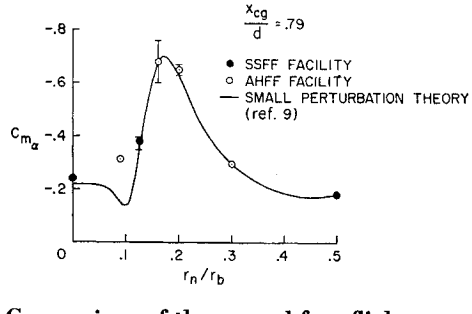

Fig. 5 Comparison of theory and free-flight experimental results on static stability for blunted 12.5° cones at $M \approx 17$.

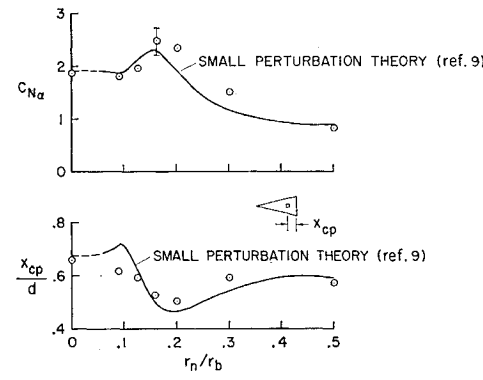

Fig. 6 Comparison of theory and experiment for normal-force-coefficient slope and center-of-pressure location at $\alpha = 0°$ for blunt 12.5° cones at $M \approx 17$.

due to viscous effects neglected in the theory. The scatter bars on the values for $r_n/r_b = 0.16$ and 0.20 indicate the estimated maximum uncertainty in the intersection of the curves with the vertical axis in Fig. 3.

Normal Force and Center of Pressure

Figure 6 shows the normal-force-coefficient slope, C_{N_α}, at $\alpha = 0°$ and the center-of-pressure location, x_{cp}/d, as functions of bluntness ratio. Measured values of C_D and C_{L_α} at $\alpha = 0°$ (see Ref. 13) were used to compute $C_{N_\alpha}(C_{N_\alpha} = C_{L_\alpha} + C_D)$ and x_{cp}/d was computed from the relation $C_{m_\alpha} = -C_{N_\alpha}[(x_{cg}/d) - (x_{cp}/d)]$, where x_{cp} and x_{cg} are measured from the model base. Also shown are theoretical predictions by the small perturbation method. Although there is some disagreement between theory and experiment, trends are similar, and the differences are such that they are self-compensating for calculating C_{m_α}. That is, for example, at $r_n/r_b = 0.3$, C_{N_α} is higher than the theory but the center-of-pressure location is also farther forward reducing the static margin. The product of the two produces a C_{m_α} value that is very close to the theoretical value as we saw earlier.

Comparison of Theories and Data for 10° Cones

As described in the introduction, other theoretical methods have been developed for predicting bluntness effects on stability. All of them have been applied to 10° half-angle cones and can therefore be directly compared, including present numerical results. Figure 7 shows the theoretical results of Clay and Walchner,[1-3] Ericsson,[6,7] and Rakich.[9] Although there are some differences especially near $r_n/r_b = 0$ and 0.35, the three theories give very similar results. Shown also are all available data for blunted 10° cones. These include the data from Refs. 2 and 12 and present results from conventional wind-tunnel tests conducted in the Ames 3.5-Foot Hypersonic Wind Tunnel at $M = 10.6$. The data for $M \approx 10$ show some scatter, but appear clearly higher than the theoretical predictions at small bluntness ratios ($r_n/r_b < 0.1$). These data were obtained over a range of Reynolds numbers from 0.18 to 1.3 million, and there is no apparent variation of static stability with Reynolds number within the scatter.

It is evident in Fig. 7 that the differences between the $M = 10$ and $M = 14$ data for a given bluntness ratio are consistent with the predicted effects of Mach number shown in Fig. 1. Where the static stability is maximum, the greater values are associated with the higher Mach numbers. At bluntness ratios of 0.3 and larger, lower values of static stability accompany the higher Mach numbers. Note, however, that the $M = 14$ wind-tunnel data agree better with the $M = 10$ theory than do the $M = 10$ data. Earlier we observed (Fig. 5) that at Mach 17 with 12.5° cones, theory and experiment

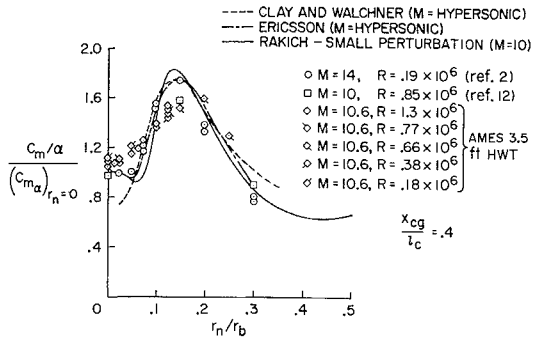

Fig. 7 Comparison of theoretical and experimental effects of nose bluntness on static stability at $\alpha = 0$ for 10° cones.

agreed. This would suggest that perhaps the agreement between theory and experiment is enhanced either by a higher Mach number or larger cone angle or both.

Figure 8 shows a comparison between the 3.5-ft wind-tunnel data and theoretical results from both small perturbation and three-dimensional characteristic calculations for normal-force-coefficient slope C_{N_α} at $\alpha = 0°$ and center-of-pressure location, x_{cp}/d, as functions of bluntness ratio. Although there is some disagreement between the theories and experiment, the trends are similar. The differences in C_{m_α} between theory and experiment at low-bluntness ratios in Fig. 7 appear to be caused principally by the differences in C_{N_α} shown in Fig. 8.

Comparisons of Theory and Experiment at Angle of Attack

The experimental data in Fig. 3 showed large variations in static stability with angle of attack. In this section we will examine the nonlinear effects of angle of attack on the static stability and compare the experimental results with theoretical calculations briefly discussed previously in the section on Theoretical Calculations.

Using the three-dimensional characteristics method, calculations were performed for angles of attack of 1° and 5° for both 10° and 12.5° cones. The results for the 10° cone at $M = 10$ are shown in Fig. 9. Plotted for each of the two angles is a parameter $(C_m/\alpha)/(C_{m_\alpha})_{r_n=0}$; that is, the pitching-moment coefficient divided by its associated value of α and normalized by C_{m_α} of the pointed cone at $\alpha = 0°$.‡ Also shown in Fig. 9 is the small perturbation curve (as shown

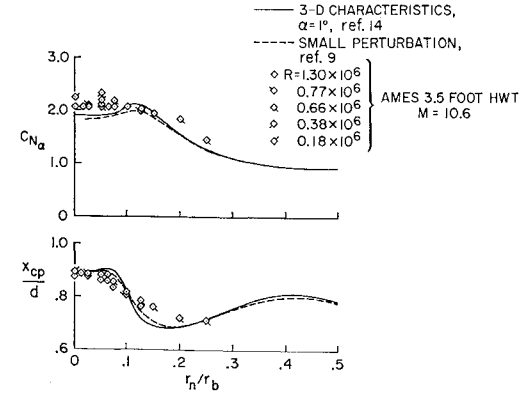

Fig. 8 Normal force coefficient slope and center-of-pressure location at $\alpha = 0°$ for blunt 10° cones.

‡ The ratio C_m/α, of course, tends to C_{m_α} as α approaches zero. It should be emphasized that this parameter is not the local slope of the pitching-moment curve unless C_m is either linear with angle of attack or α is very near 0.

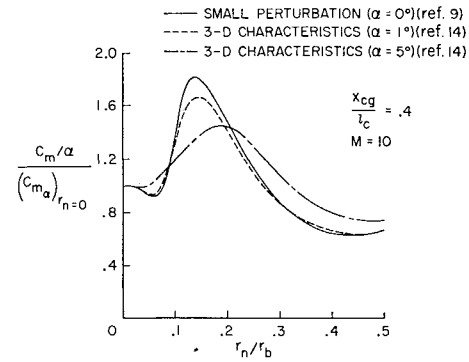

Fig. 9 Theoretical calculations of static stability for blunt 10° cones for several angles of attack.

in Fig. 7) for $\alpha = 0$. These small perturbation results agree with those from the three-dimensional characteristics solution for $\alpha = 1°$ except for the region near maximum stability. The general three-dimensional method of characteristics program is believed to be the more accurate of the two methods. It should be noted, however, that the peak value of C_{m_α} may be sensitive to the size of the finite difference mesh. The general program was run with only one mesh size, 15 points between the body and shock wave on 7 meridional planes. Numerical results with this mesh size agree with experimental pressures[14,19] for bluntness ratios greater than $r_n/r_b = 0.08$ and to angles of attack up to approximately 10°.

In Fig. 10, the parameter C_m/α for 12.5° cones at $M = 17$ has been plotted for both $\alpha = 1°$ and $\alpha = 5°$ along with the small perturbation curve shown earlier in Figs. 1 and 5. The 3-D characteristics curve for $\alpha = 1°$ agrees with the small perturbation curve except in the regions near the minimum and the peak. The most significant fact is that at $\alpha = 5°$ theory and experiment are in good agreement just as they were for $\alpha = 0°$. (The experimental data points for $\alpha = 5°$ were obtained in the same manner as were the theoretical. The value of C_m at $\alpha = 5°$, shown in Fig. 4, was divided by 5° and multiplied by 57.3 to express the result in radians^{-1}.) The good agreement at both $\alpha = 0°$ and $\alpha = 5°$ indicates that the theory is yielding accurate results in the small angle-of-attack range. Values of C_m/α (actually C_{m_α} since $\alpha = 0°$) for 12.5 cones based on Ericsson's hypersonic theory[7] are also shown. Values using Ericsson's theory were calculated at six bluntness ratios ($r_n/r_b = 0.004, 0.05, 0.10, 0.15, 0.2, 0.3$) and a curve faired through these points is shown. Although there are some small differences in the low-bluntness region, the agreement is quite good, especially with the three-dimensional characteristics method for $\alpha = 1°$.

Conclusions

Free-flight tests of blunted 12.5° cones at $M = 17$ to 18 and conventional wind-tunnel tests for 10° cones at $M =$

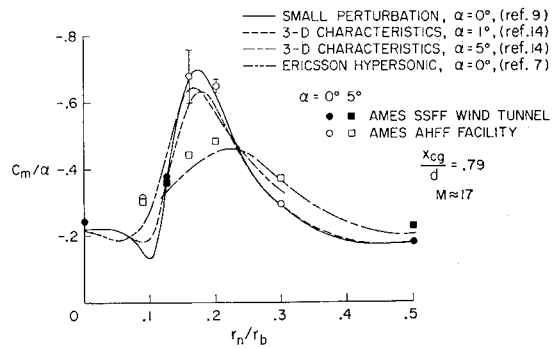

Fig. 10 Comparison of static-stability theory and experiment for blunt 12.5° cones at several angles of attack.

10.6 along with recent theoretical calculations studied to determine the aerodynamic effects of bluntness on slender cones have indicated the following significant conclusions.

1. The strong dependence of initial moment-curve slope on nose bluntness for slender angle cones as predicted by several recent theories and shown previously at Mach numbers generally near $M = 10$, is found to occur experimentally at a Mach number of 17 and is, if anything, more pronounced at this higher Mach number.

2. The method of characteristics predicts this effect with relatively good accuracy, both at zero angle of attack and angles up to 5°. Some local and presently unexplained disagreements between characteristics theory and experiment occur, principally with small ratios of nose radius to base radius (<0.1).

3. Other more approximate theories also give good agreement with characteristics theory and experiment, including Ericsson's theory based on the embedded Newtonian flow except and Clay and Walchner's empirical correlation.

4. Strong nonlinearities in the pitching-moment curve with angle of attack occur with blunted cones, and the static stability diminishes with increasing angle at small nose bluntness and increases with increasing angle at large nose bluntness.

References

[1] Clay, J. T. and Walchner, O., "Nose Bluntness Effects on the Stability Derivatives of Cones in Hypersonic Flow," *Transactions of the Second Technical Workshop on Dynamic Stability Testing*, Arnold Air Force Station, Tenn., Vol. I, Paper 8, April 20–22, 1965.

[2] Clay, J. T., "Nose Bluntness, Cone Angle, and Mach Number Effects on the Stability Derivatives of Slender Cones," Sept. 1967, ARL 67-0185, Wright-Patterson A. F. Base, Ohio.

[3] Walchner, O., "Research on Hypersonic Stability Derivatives in Pitch for Blunted Slender Cones," *Research Review*, Vol. VII, No. 2, Feb. 1968, Office of Aerospace Research, U. S. Air Force. Arlington, Va.

[4] Griffith, B. J. and Lewis, C. H., "A Study of Laminar Heat Transfer to Spherically Blunted Cones and Hemisphere-Cylinders at Hypersonic Conditions," TDR 63-102, June 1963, Arnold Engineering Development Center, Arnold Air Force Station, Tenn.

[5] Cheng, H. K., "Hypersonic Flow with Combined Leading Edge Bluntness and Boundary Layer Displacement Effect," AF-1285-A-4, Aug. 1960, Cornell Aeronautical Lab., Buffalo, N. Y.

[6] Ericsson, L. E. and Scholnick, I. M., "Effect of Nose Bluntness on the Hypersonic Unsteady Aerodynamics of Flared and Conical Bodies of Revolution," *Journal of Spacecraft and Rockets*, Vol. 6, No. 3, March 1969, pp. 321–324.

[7] Ericsson, L. E., "Hypersonic Unsteady Aerodynamics of Blunted Slender Cones at Moderate Attitudes," 6-R1-69-1, Oct. 1969, Lockheed Missile & Space Co., Sunnyvale, Calif.

[8] Seiff, A., "Secondary Flow-Fields Embedded in Hypersonic Shock Layers," TN D-1304, May 1962, NASA.

[9] Rakich, J. V., "Calculation of Hypersonic Flow Over Bodies of Revolution at Small Angles of Attack," *AIAA Journal*, Vol. 3, No. 3, March 1965, pp. 458–464.

[10] Brong, E. A., "The Unsteady Flow Field About a Right Circular Cone in Unsteady Flight," FDL-TDR-64-148, Jan. 1967. Air Force Flight Dynamics Lab, Wright-Patterson A. F. Base, Ohio.

[11] Rie, H., Linkievicz, E. A., and Bosworth, F. D., "Hypersonic Dynamic Stability, Part III, Unsteady Flow Field Program," FDL-TDR-64-149, Jan. 1967, Air Force Flight Dynamics Lab, Wright-Patterson A. F. Base, Ohio.

[12] Ward, L. K. and Uselton, B. L., "Dynamic Stability Results for Sharp and Blunted 10-Deg. Cones at Hypersonic Speeds," *Transactions of the 3rd Technical Workshop on Dynamic Stability Problems*, NASA Ames Research Center, Moffett Field, Calif., Vol. III, Paper 2, Nov. 4–7, 1968.

[13] Malcolm, G. N. and Rakich, J. V., "Comparison of Free-Flight Experimental Results with Theory on the Nonlinear Aerodynamic Effects of Bluntness for Slender Cones at Mach Number 17," AIAA Paper 70-554, Tullahoma, Tenn., 1970.

[14] Rakich, J. V., "A Method of Characteristics for Steady Three-Dimensional Supersonic Flow with Application to Inclined Bodies of Revolution," TN D-5341, Oct. 1969, NASA.

[15] Malcolm, G. N. and Chapman, G. T., "A Computer Program for Systematically Analyzing Free-Flight Data to Determine the Aerodynamics of Axisymmetric Bodies," TN D-4766, 1968, NASA.

[16] Nicolaides, J. D., "On the Free-Flight Motion of Missiles Having Slight Configurational Asymmetries," Rept. 858, 1953, Ballistics Research Lab., Aberdeen Proving Ground, Md.

[17] Rasmussen, M. L. and Kirk, D. B., "On the Pitching and Yawing Motion of a Spinning Symmetric Missile Governed by an Arbitrary Nonlinear Restoring Moment," TN D-2135, 1964, NASA.

[18] Malcolm, G. N., "Stability and Drag Characteristics at Mach Numbers of 10 and 26 of a Proposed Slender Atmospheric Probe," TN D-3917, 1967, NASA.

[19] Rakich, J. V. and Clearly, J. W., "Theoretical and Experimental Study of Supersonic Steady Flow Around Inclined Bodies of Revolution," *AIAA Journal*, Vol. 8, No. 3, March 1970, pp. 511–518.